SENSOR SYSTEMS FOR SHM

Comprehensive structural monitoring can be realized only if the monitored structure is instrumented with arrays of sensor systems at critical locations throughout the structure. At the same time, it is implausible to expect that one type of sensors alone would be able to track down the complete structural behaviour as well as detect all possible structural abnormalities. Hence, comprehensive monitoring calls for deploying complementary sensor systems with sufficient redundancy, so that a few sensors could be allowed to fail without triggering total collapse of the monitoring system (Boller, 2002). Besides, the sensors and the associated data collection systems should be capable of withstanding the harsh conditions encountered in the underground structures during construction and operation.

In general, sensors used for SHM can be classified as the surface type and the embedded type. The surface type sensors can be replaced if they tend to become faulty at any stage. However, there is very limited possibility of repair or replacement for the embedded sensors. Hence, the embedded sensors should be exceptionally robust and durable. The following parts of this section cover the operating principles of various sensing systems, which could possibly be deployed for monitoring underground structures. Their pros and cons are highlighted with regard to the underground conditions.

2.1 Strain Gauges

Strain gauges are very versatile sensors for structural behaviour monitoring. Strains on structural surfaces are caused by complex member deformations, resulting from bending, torsion, shearing and elongation/ contraction. Hence, strain measurements can capture an element's behaviour quite well (Sanayei et al., 1996). For efficient performance, it is desirable that the gauge should be stable with respect to both time and temperature. In addition, it should have minimum dimensions and inertia and should exhibit linear response over the strain range of interest (Dally et al., 1984). Commercial strain gauges are available in various types, based on mechanical, electrical or optical principle. Described below are prominent types of strain gauges available commercially.

2.1.1 Vibrating Wire Strain Gauge (VWSG)

Fig. 3 shows the details of a typical VWSG. A VWSG essentially consists of a pretensioned stainless steel wire, with its ends fixed to lugs that are spot-welded to the

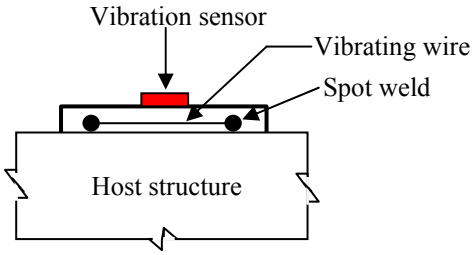

Fig. 3 A vibrating wire strain gauge.

monitored component. A sensor coil, positioned over the wire, when energized, plucks the wire and measures the frequency of the resulting vibrations. The natural frequency of vibration, f, is related to the tension F in the wire by

$$f = \frac{1}{2l}\sqrt{\frac{F}{m}} \tag{1}$$

where l represents the length of the wire and m the mass per unit length. Any change in the strain, $\Delta\varepsilon$, from the original condition, causes a change in the tension by ΔF and hence alters the natural frequency by Δf. For small strain, using Hooke's law, the change in strain can be expressed as (Batten et al., 1999)

$$\Delta\varepsilon = \left(4l^2\frac{m}{YA}\right)(\Delta f)^2 \tag{2}$$

where Y is the Young's modulus of the wire and A its cross-sectional area.

If VWSGs are employed for long term monitoring of structural components, which are likely to be subjected to temperature fluctuations, care should be exercised in interpreting their readings. For temperature change of ΔT, if the structural component and the VWSG have the same coefficient of thermal expansion, α, and if the monitored component is unrestrained, each will undergo free thermal expansion strain $\alpha\Delta T$, causing no stress, either in the component or the VWSG. Consequently, the reading of the VWSG will not undergo any change. If now an external load be superimposed, the strain will develop purely due to the applied load. Hence, in real situation where the two effects are superimposed, the VWSG will only capture the strain resulting from the actual load in the member. Thus, no correction is necessary in the strain measured by the VWSG if the coefficient of thermal expansion of the monitored component is same as that of the VWSG. However, if the coefficient of thermal expansion of the monitored component is different, say β, and if the component is unrestrained, a strain equal to $(\beta - \alpha)\Delta T$ will develop in the VWSG (and will be indicated by it). This is spurious, since it does not cause any stress in the monitored component. Hence, in

general, when load (or constraints) and temperature fluctuation occur concurrently, the measured strain ε_m should be corrected as

$$\varepsilon_{corr} = \varepsilon_m - (\beta - \alpha)\Delta T \tag{3}$$

VWSGs are structurally strong and quite robust for use in underground structures. They are especially suitable for long term monitoring since vibration wires do not undergo any decay with time (Oosterhout, 2003). They can be easily spot welded to the reinforcement bars of the reinforced concrete structural members. This instrumentation technique was adopted in the bridge linking Singapore and Malaysia, which was extensively instrumented with VWSGs during construction in 1997 (Moyo, 2002). The installed VWSGs are still operational, even after seven years. Oosterhout (2003) reported a similar monitoring program for underground structures, primarily based on VWSGs, spanning five years. This clearly demonstrates the robustness and longevity of VWSGs

The main drawback of VWSGs is that they are only suitable for measuring static strains since they require plucking of the wire. They are also susceptible to extraneous noise in the form of ambient vibrations. If installed externally (such as on steel struts used for supporting temporary retaining walls in deep excavations), special protection is needed to prevent damage from routine construction activities carried out in the vicinity.

2.1.2 Electrical Strain Gauge (ESG)

ESGs are based on the principle that under mechanical stress, the electrical resistance of a conductor changes in proportion to the load induced strain. They essentially consist of thin metallic foil grids, bonded to a thin, tough and flexible polyimide plastic film, which can be adhesively bonded to the surface of the monitored component, as shown in Fig. 4(a). The polyimide film provides electrical insulation between the gauge and the monitored component. When the structural component is loaded, its strain is transferred to the foil grid and its resistance changes accordingly. The relative change in resistance, $\Delta R/R$ of the foil, is related to the strain ε by (Dally et al., 1984)

$$\frac{\Delta R}{R} = S_g \varepsilon \tag{4}$$

where S_g is called the gauge factor or the calibration constant of the ESG. It varies between 2 and 4 for most alloys used in strain gauge fabrication, such as constantan, karma and nichrome. The output $\Delta R/R$ of a strain gauge is converted into voltage signal by means of a Wheatstone bridge circuit, as shown in Fig. 4(b). For this circuit, the output voltage V_o is given by

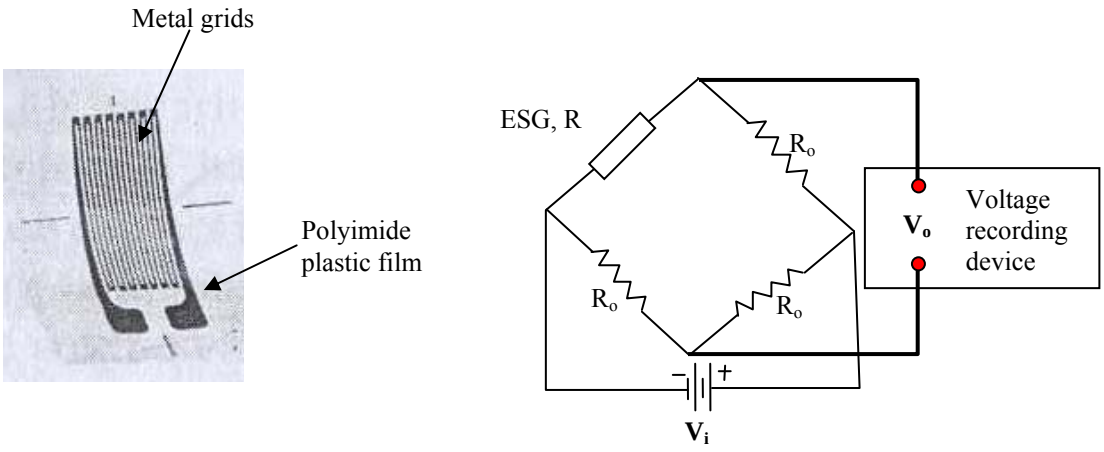

Fig. 4 (a) An electrical strain gauge foil.
(b) A Wheatstone bridge circuit.

$$V_o = \frac{1}{4} V_i \left(\frac{\Delta R}{R} \right) = \frac{1}{4} V_i S_g \varepsilon \tag{5}$$

The input voltage, V_i, is governed by the power that can be dissipated by the gauge, that in turn depends on the gauge length (0.2-100mm) and the initial resistance of the gauge. The output voltage usually ranges between 1 and 10μV per micro unit of strain.

Like VWSG, the strain measured by an ESG also needs to be compensated against temperature. A temperature change causes change in S_g as well as a change in the original gauge resistance (R), in addition to causing the spurious strain equal to $(\beta - \alpha)\Delta T$. The temperature related changes in S_g are very small, usually less than 1% for a temperature variation of 100°C. Hence, they can be neglected in routine stress analysis, unless temperature variations of several hundred degrees are expected. The other effects, if combined, lead to a spurious change in the resistance of the gauge, given by

$$\left(\frac{\Delta R}{R} \right)_{spurious} = (\beta - \alpha) S_g \Delta T + \gamma \Delta T \tag{6}$$

where γ is the temperature coefficient of resistivity of the gauge alloy. A temperature compensated gauge can be obtained if both the terms in Eq. (6) are zero or cancel each other. However, such temperature compensation is rarely possible and that too over narrow

temperature ranges only. Hence, in general, corrections need to be made by subtracting Eq. (6) from the measured $\Delta R/R$ (Eq. 5).

ESGs need considerable care during installation due to their fragile nature. Further, electrical noise is very frequently associated with ESGs since the output voltage from a Wheatstone bridge is of the order of few milli volts only. Fortunately, electrical noise can be substantially reduced by employing twisted leads with a properly grounded shield (Dally et al., 1984). In addition, ESGs are very prone to deterioration by water. This problem is was experienced during the monitoring of rock bolts in the underground caverns in Singapore (Zhao et al., 2002). Hence, they must be properly sealed if used in the underground structures, where they are likely to encounter excessive dampness. In general, ESGs tend to be less stable as compared to VWSGs over long periods of time. Because of this reason, majority of the long-term studies reported in the literature have deployed VWSGs rather than ESGs.

2.1.3 Optical Fibre Bragg Grating (FBG) Based Strain Gauges

Optical fibres, which are thin fibres (few μm to few hundred μm in diameter) of glass and silica, utilize fibre properties to generate optoelectronic signals indicative of the external parameters to be measured. Though originally developed for telecommunication purposes, they have found tremendous recognition as sensors since the 1990s. Of the various available fibre optic technologies, FBG has proven to be most versatile (Tjin et al., 2002). A Bragg grating is a periodic structure, fabricated by exposing a photosensitised fibre to an ultraviolet light, as shown in Fig. 5. After fabrication, when light from a broad band source interacts with the grating, a single wavelength, known as Bragg wavelength, is reflected back while the rest of the signal is transmitted. The Bragg wavelength, λ_B, is related to the grating pitch Λ and the effective refractive index n_{eff} of the grating by

$$\lambda_B = 2\Lambda n_{eff} \tag{7}$$

Any mechanical strain in the fibre will shift the Bragg wavelength through expansion/ contraction of the grating periodicity and the photo elastic effect. Similarly, temperature variation causes thermal expansion/ contraction of the grating periodicity and also the refractive index. These effects provide the means of employing the FBG written fibres as the sensor elements for measuring strains and temperatures. The change in Bragg wavelength due to an external disturbance, comprising a strain change $\Delta\varepsilon$, a temperature change ΔT and a pressure change ΔP, can be quantitatively expressed as

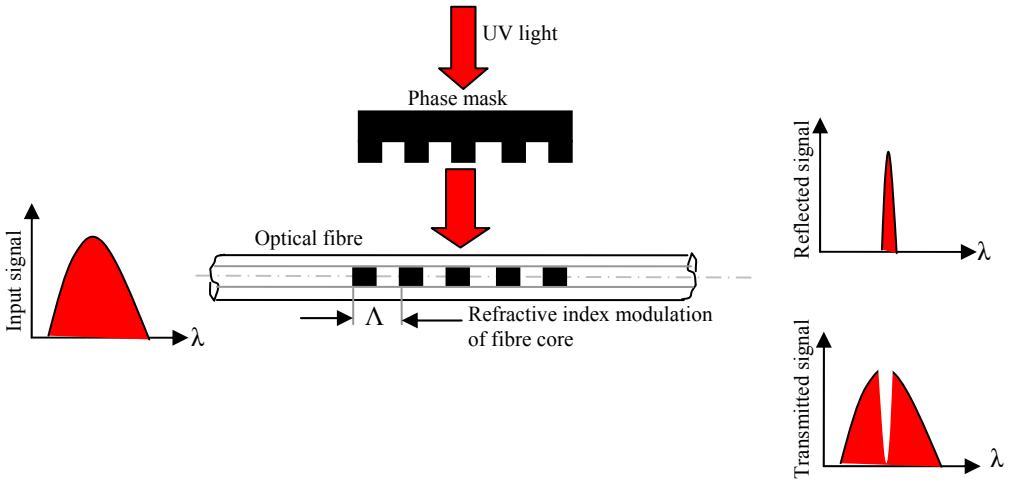

Fig. 5 Fabrication and principle of FBG sensors.

$$\frac{\Delta\lambda_B}{\lambda_B} = K_\varepsilon \Delta\varepsilon + K_T \Delta T + K_P \Delta P \tag{8}$$

where K_ε, K_P and K_T and are the wavelength sensitivity coefficients to strain (ε), temperature (T) and pressure (P) respectively. Thus, to be used as strain sensor (in the absence of pressure), the measured strain needs to be corrected for temperature. Usually, this is achieved by installing an additional FBG close to the strain sensing FBG, but not bonded to the structure. This measures the wavelength shift on account of temperature alone, which can then be compensated. In addition, as in the case of VWSG and ESG, the spurious strain $(\beta - \alpha)\Delta T$, due to differential thermal expansions of the fibre and structure, also need to be eliminated from the measured strain.

A comprehensive research programme is underway at Nanyang Technological University (NTU), Singapore, for the development of cost-effective and durable FBG based sensors for civil-structural applications (Ng et al., 1998; Tjin et al., 2001, 2002; Brownjohn et al, 2003a). The strain sensor developed at NTU consists of an FBG, about 10mm long, sandwiched between carbon composite layers (50mm long and 0.5mm thick), as shown in Fig. 6. Experimental evaluation of this FBG sensor on lab sized structures by Moyo (2002) through static and dynamic tests indicated good possibility of its use on civil structures. Many other applications of FBG sensors on ground based structures have been reported (Storoy et al., 1997; Tjin et al., 2002). Liu et al. (2002) recently demonstrated feasibility of their application in monitoring underground structures.

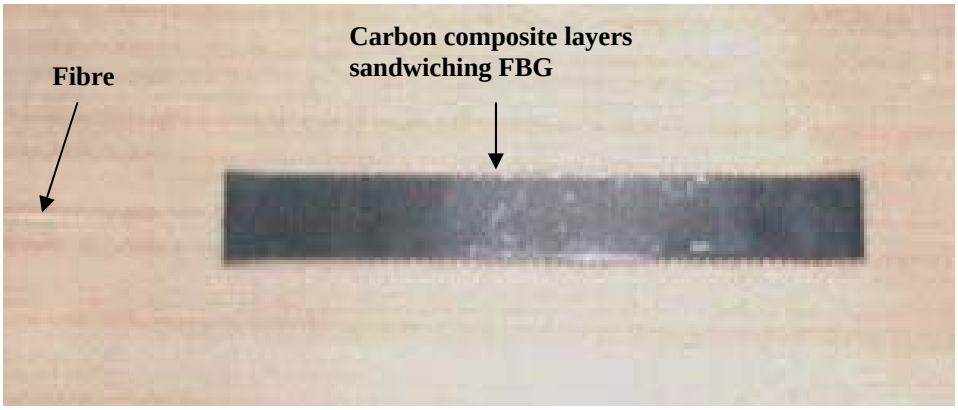

Fig. 6 FBG based strain sensor developed at NTU (Moyo, 2002)

FBG sensors are small, lightweight, corrosion resistant and durable. VWSGs and ESGs require cables for recording data, which, for long distance monitoring, suffer from electro-magnetic interference and electrical noise. FBG sensors, on the other hand, are immune to EMI and can be multiplexed, thus eliminating long cables. However, they are very fragile as compared to VWSGs and ESGs. For this reason, efforts to install FBG sensors on civil structures often result in high rate of sensor failure due to the harsh environment in the construction industry (e.g. Storoy et al., 1997). They have yet to fully mature in terms of standard field proven devices like the ESGs and the VWSGs. In addition, the measurement system and the sensors themselves are relatively expensive as compared to the conventional sensor systems.

2.2 Extensometers

Extensometers are devices commonly employed in underground structures, especially newly created rock caverns, for measuring displacements resulting from excavations. Extensometers are of two types- tape extensometers and multiple point borehole extensometers.

A tape extensometer consists of a telescopic rod, an invar bar, and a tape under constant tension, placed between two measuring points on the rock surface, such as a rock cavern. Hence, it measures the relative displacements (convergence/ divergence) between the two points. A portable dial gauge is generally employed to record the convergence data. Fig.

7 shows a typical section for convergence measurement in a tunnel/ cavern (Zhao et al., 2002). The nature of displacements depends on the relative magnitude of the horizontal and the vertical stresses. If horizontal stresses are higher than the vertical stresses, the roof of the tunnel/ cavern moves up and the sides move inwards. On the other hand, if vertical stresses are higher than the horizontal stresses, the roof moves downwards and the side walls are displaced outwards. If convergence measurements are recorded along all sides of a triangle, then it is possible to derive the absolute measurements from trigonometric principles. For example, in triangle 124 of Fig. 7, if the absolute measurements (normal to tunnel/ cavern boundary) are u_1, u_2 and u_4 respectively at points 1, 2 and 4 respectively (positive if inwards), then these can be related to the measured convergence by

$$\delta_{14} = u_1 + u_4 \tag{9a}$$

$$\delta_{12} = u_1 \cos\theta_1 + u_2 \cos\theta_{21} \tag{9b}$$

$$\delta_{24} = u_4 \cos\theta_4 + u_2 \cos\theta_{24} \tag{9c}$$

where δ_{ij} represents the measured convergence between points i and j. Hence, from this set of algebraic equations, if the angles θ_1, θ_2, θ_{21} and θ_{24} are known, the absolute displacements u_1, u_2 and $u_{4\,can}$ be determined.

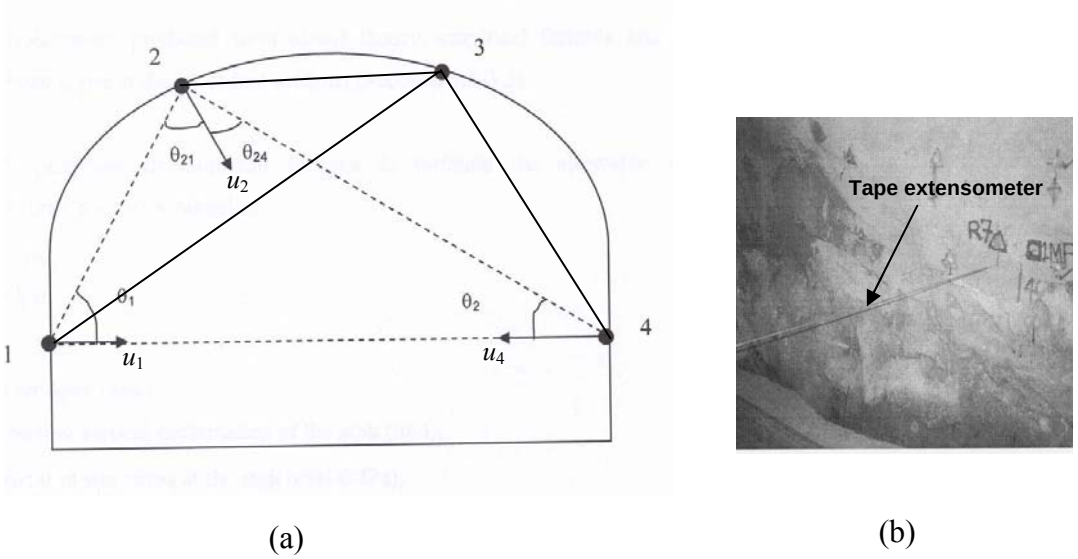

(a) (b)

Fig. 7 (a) Tunnel section instrumented with six tape extensometers.
(b) A close up view of a tape extensometer.

Tape extensometers were extensively employed for monitoring of large caverns in Singapore (Zhao et al., 2002). The measured displacements helped the specialists in deciding whether the excavations are safe or they require additional strengthening. The main limitation of the extensometers is that they entail manual recording of data, which could be tedious. Besides, slight loosening of convergence pins can severely affect the accuracy of the measurement results. In addition, instrumenting a particular section disrupts movement across the section.

Multiple point borehole extensometers work on a principle similar to the tape extensometers but they can measure the relative displacements between several points, at various depths in a borehole. Hence, the multiple point borehole extensometers can provide the distribution of displacements in relatively large volumes of rock. Fig. 8 shows a typical cavern cross section instrumented with borehole extensometers (Zhao et al., 2002). Such borehole extensometers were extensively employed in Singapore for assessing the stability of newly excavated caverns. Generally, the farthest anchor of the extensometer (usually about 12-25m inside rock) is assumed non-movable. Hence, the recorded displacements are taken as absolute displacements. However, this assumption is no longer valid if there are deep seated movements along fractures, which was the case experienced by Zhao et al. (2002).

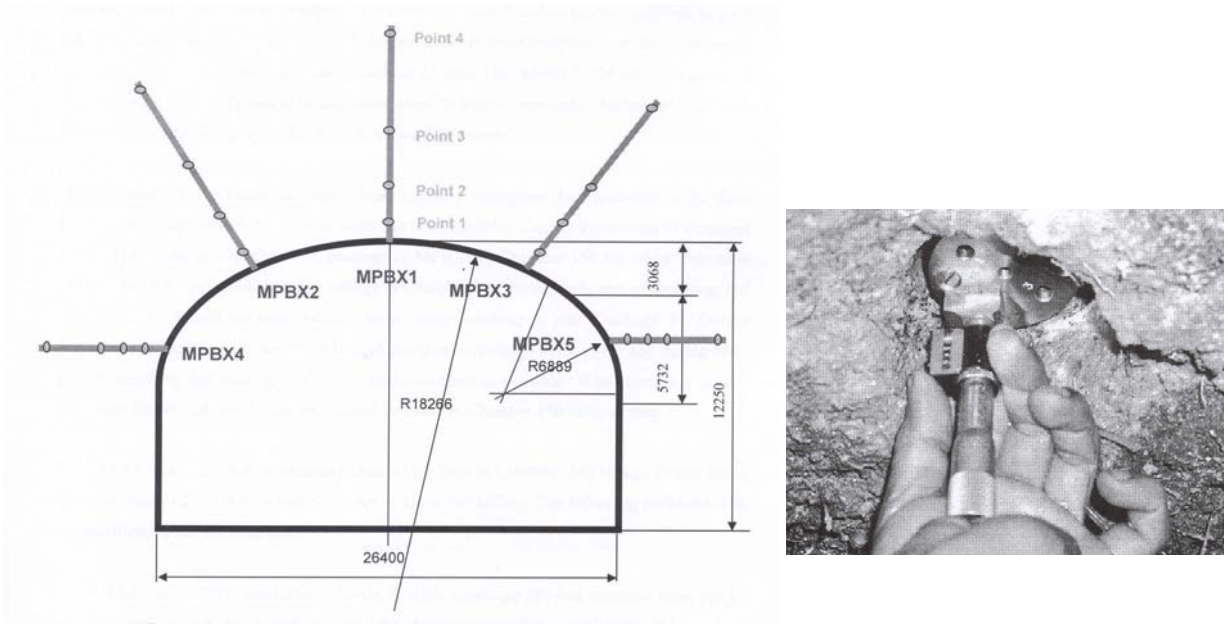

(a) (b)

Fig. 8 (a) Tunnel section instrumented with five borehole extensometers.
(b) A close up view of a borehole extensometer.

2.3 Accelerometers

Accelerometers are employed for measuring dynamic responses of structures. The response can be either harmonic (e.g. dynamic vibration tests) or transient (e.g. earthquake response). An accelerometer essentially consists of a seismic mass connected to a base (which is attached to the host structure) by means of a spring and a viscous damper. The working principle of an accelerometer is depicted in Fig. 9, which shows the seismic mass m connected to a base mass m_b by a spring (of spring constant k) and a damper (with a damping constant c). Let x, $\dot{x}$ and $\ddot{x}$ denote the displacement, velocity and acceleration respectively of the base and y, $\dot{y}$ and $\ddot{y}$ represent the corresponding terms for the seismic mass. Using Newton's second law, the equation of motion of the seismic mass can be written as

$$m\ddot{y} + c(\dot{y} - \dot{x}) + k(y - x) = F(t) \tag{10}$$

where $F(t)$ denotes the external force imposed upon the transducer. Substituting $y - x = z$, $\dot{y} - \dot{x} = \dot{z}$ and $\ddot{y} = \ddot{x} + \ddot{z}$, in the absence of an external force (i.e. $F(t) = 0$), Eq. (9) can be reduced to

$$m\ddot{z} + c\dot{z} + kz = -m\ddot{x} \tag{11}$$

If the base motion is harmonic in nature, i.e. $x = x_o e^{j\omega t}$, the governing differential equation (Eq. 10) can be rewritten as

$$m\ddot{z} + c\dot{z} + kz = m\omega^2 x_o e^{j\omega t} \tag{12}$$

The general solution for Eq. (12) can be derived as (Clough and Penzien, 1993)

$$z = \frac{m\omega^2 x_o}{k\sqrt{(1-r^2)^2 + (2r\xi)^2}} e^{j(\omega t - \phi)} \tag{13}$$

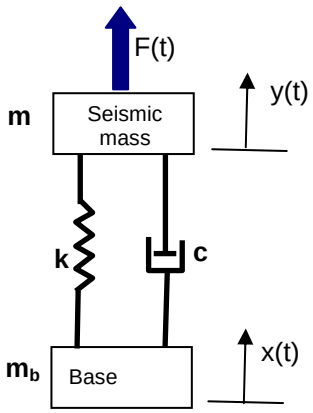

Fig. 9 Working principle of an accelerometer.

where r denotes the ratio of the excitation frequency and the natural frequency, i.e. (ω/ω_n) and $\xi = c/2\sqrt{km}$ represents the dimensionless damping ratio. ϕ is the phase lag of z behind x, as given by

$$\tan\phi = \frac{2r\xi}{1-r^2} \tag{14}$$

Since $\ddot{x} = -\omega^2 x_o e^{j\omega t}$, and $\omega_n = \sqrt{k/m}$, Eq. (13) can be further simplified as

$$z = \left(\frac{-e^{-j\phi}}{\omega_n^2 \sqrt{(1-r^2)^2 + (2r\xi)^2}} \right) \ddot{x} \tag{15}$$

where $\omega_n = \sqrt{k/m}$ is the natural frequency of the transducer system. For the limiting case of very small frequency ratios (i.e. $\omega << \omega_n \Rightarrow r \to 0$ and $\phi \to 0$), Eq. (15) can be simplified as

$$\ddot{x} \approx -z\omega_n^2 \tag{16}$$

Hence, the acceleration of the host system can be determined by measuring the relative displacement, z, between the seismic mass and the base. In order to ensure the necessary condition $\omega << \omega_n$, the system has to be equipped with very stiff springs and a small seismic mass. Most commercial accelerometers employ piezoelectric transducers as displacement sensors due to their small mass, high stiffness and low damping. However, since the piezoelectric sensing elements are charge generating elements, high input impedance signal conditioning instruments, such as charge amplifiers, integrated circuit amplifiers or voltage followers must be incorporated in the circuit to convert the acceleration induced charge into an output voltage that can be measured and recorded. For measuring transient signals, the natural time period of the transducer should be sufficiently smaller than the rise time of the input signal (preferably by less than one fifth). Otherwise, the transducer response will be severely distorted. Similarly, the electrical time constant of the system must be sufficiently large to prevent serious signal delays during a transient event, such as an earthquake.

The drawbacks of the present day accelerometers include small bandwidth, bulkiness, high cost and susceptibility to mechanical and electrical noise. New types of accelerometers, based on microelectromechanical systems (MEMS) technology, have recently been reported (Lynch et al., 2003), but yet to be commercialized. These promise a higher operational bandwidth, low noise and superior performance, including wireless data transmission and recording.

2.4 Pressure Transducers

Most pressure transducers measure pressure indirectly, through the measurement of the associated strains or displacements. Diaphragm type pressure transducers are the most commonly used in several industries. These consist of a clamped circular plate, as shown in Fig. 10(a), which acts as a diaphragm. When a uniform pressure is applied normal to the diaphragm, it develops radial and circumferential strains, directly proportional to the applied pressure (provided the deflection is small, less than one-fourth of the diaphragm thickness). For an applied pressure p, the radial strain, ε_{radial}, and the circumferential strain, ε_{circum}, can be expressed as (Dally, 1984)

$$\varepsilon_{radial} = \frac{3p(1-\nu^2)(R^2-3r^2)}{8Yt^2} \qquad \varepsilon_{circum} = \frac{3p(1-\nu^2)(R^2-r^2)}{8Yt^2} \tag{17}$$

where R is the diaphragm radius, r the position parameter, t the diaphragm thickness, ν the Poisson's ratio and Y the Young's modulus of the diaphragm. The strains are measured using specially designed ESGs, instrumented on the diaphragm as shown in Fig. 10(b). Radial ESGs are instrumented near the edges and circumferential ESGs near the centre of the diaphragm. The ESGs are connected to a Wheatstone bridge circuit, which produces an output voltage proportional to the averaged strain. Pressure can be expressed in terms of the ratio of the output voltage to the input voltage, V_o/V_i , of the Wheatstone bridge as

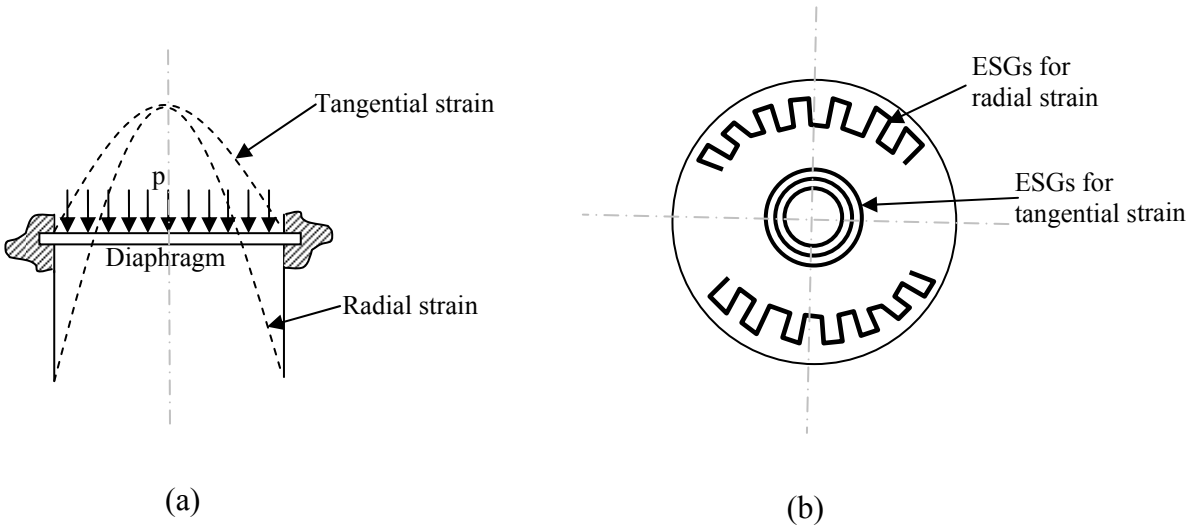

Fig. 10 (a) Diaphragm type pressure gauge.
(b) Special ESGs installed on diaphragm.

$$p = \frac{1.22Yt^2}{R^2(1-\nu^2)}\left(\frac{V_o}{V_i}\right) \tag{18}$$

The voltage sensitivity of the pressure transducer can be increased by increasing the ratio *R/t*. However, this is limited by diaphragm deflection, which must be smaller than *t/4* in order for Eq. (16) to be valid.

These type of transducers can measure pressures up to 200 MPa. For higher pressures, hollow cylinders are employed instead of diaphragms, whose measurement range is as high as 700 MPa. The diaphragm type pressure transducers can measure static as well as dynamic pressures up to 10 kHz frequencies.

Another type of pressure transducer employs quartz, a piezoelectric crystal, for sensing pressures. The quartz crystal is enclosed in a cylindrical shell, fitted with a pressure transmitting diaphragm at one end and a rigid base at the other, as shown in Fig. 11. An electrostatic charge Q is generated when a pressure p is applied on the diaphragm, as given by

$$Q = d_{33} pA \tag{19}$$

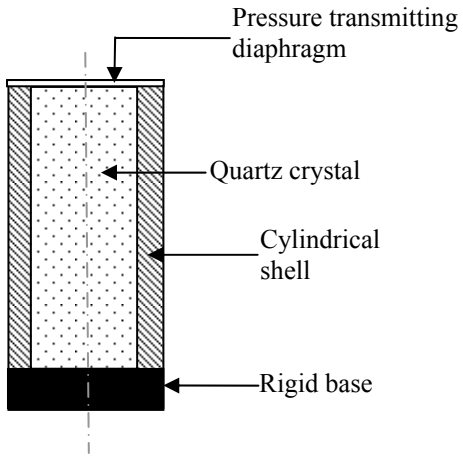

Fig. 11 Piezoelectric type pressure transducer.

where d_{33} is the piezoelectric constant of quartz and A the area of the crystal. Commercial piezoelectric stress transducers exhibit charge sensitivities, ranging from 150pC/MPa to 700 pC/MPa. Because piezoelectric crystals exhibit extremely high output impedance, the charge generated is measured using a circuit that includes a charge amplifier inserted between the transducer and the voltage measuring instrument. The charge amplifier converts the pressure generated charge into an amplified voltage and provides an output impedance of 100Ω, which suits most commercial voltage measuring instruments. The quartz based pressure transducers can measure quasi static and dynamic pressures up to 700 MPa. Quartz is characterized by a high modulus of elasticity, high resonant frequency (250-500 kHz), negligible ageing effects and very low hysteresis. Hence, the frequency bandwidth of the piezoelectric based pressure transducers is much higher than the diaphragm type pressure transducers.

Besides the diaphragm type and the piezoelectric type pressure transducers, FBG based pressure sensors have recently been conceptually developed and tested at NTU (Tjin et al., 2001). However, the FBG based pressure sensors need to be field tested before they can be commercialized.

Pressure transducers were employed by Moyo (2002) for monitoring concrete stresses in the bridge linking Singapore and Malaysia, during its construction and operation. It was reported that after the curing of concrete, the stress cells demanded repressurisation, to re-establish contact with the surrounding concrete. Hence, they could only measure the relative and not the absolute concrete stresses. Oosterhout (2003) employed liquid type pressure transducers, consisting of a mercury filled reservoir, enclosed by a diaphragm, as embedded transducers for concrete. The diaphragm strain was in turn measured by a vibrating wire. However, the researchers reported problems with this type of pressure transducers, especially in the form of strong temperature dependence of the measurements.

2.5 Temperature Sensors

Temperature monitoring is very crucial in understanding the environmental effects on structural responses. In overall SHM, monitoring temperature variations helps in separating the effects of environment from those due to imposed loads, damages and other serious anomalies. In addition, as mentioned before, measurements of the ESGs, the VWSGs and the FBG based sensors need to be corrected for temperature fluctuations. This necessitates measuring temperature accurately along with strains and pressures.

In practice, temperature can be measured by monitoring change in the volume of a liquid, change in the length of a bar, change in the electrical resistance of a conductor and

change in the pressure of a gas at constant volume. Following sections briefly describe the common commercial temperature sensors based on these principles.

2.5.1 Expansion Thermometers

The expansion type thermometers are based on the principle that a structural component undergoes change in dimensions with a temperature change ΔT according to

$$\frac{\Delta L}{L} = \alpha \Delta T \tag{20}$$

where α is the coefficient of thermal expansion, L the original length of the component and ΔL the change in length on account of temperature variation. However, due to the small value of α, accurate measurement of ΔL is very difficult. This difficulty is overcome by utilizing the differential expansion of two materials. The *liquid-in-glass* thermometer is one such thermometer, wherein a bulb holds a liquid such as mercury or alcohol. When subjected to temperature change, both the bulb and the fluid undergo volume change. The differential volume change, which is directly proportional to temperature change, is indicated by an indexed capillary tube. Although inexpensive, visual readout limits the applicability of the liquid-in-glass thermometers for automated SHM. Alternatively, the tube could be closed and the pressure developed could be transmitted to a pressure transducer. This type of thermometer is called *pressure thermometer* and can enable automatic measurements. However, its response to dynamic temperature variations is not so good. *Bimetallic thermometer*, another expansion type thermometer, consists of a bonded composite of two metals, one with large α (such as copper), and the other with small α (such as invar). When subjected to temperature change, the differential expansion causes the strip to bend into a circular arc, whose radius of curvature provides the measurement of the temperature. In spite of simplicity, most expansion type thermometers are somewhat bulky and not suitable for long term temperature measurements in the underground structures.

2.5.2 Resistance Temperature Detectors (RTD)

An RTD consists of a resistive element (such as platinum, nickel or nickel-copper alloy), that undergoes change in resistance with temperature in accordance with

$$R = R_o(1 + \gamma_1 \Delta T + \gamma_2 \Delta T^2 + ... + \gamma_n \Delta T^n) \tag{21}$$

where γ_i are the temperature coefficients of resistivity and R_o the resistance at the reference temperature. The number of terms in Eq. (20) depends upon the material, the temperature

range and the accuracy desired. For the typical temperatures encountered in civil-structures and for practical reasonable accuracy, Eq. (21) can be simplified as

$$\frac{\Delta R}{R} = \gamma(T - T_o) \tag{22}$$

where $\Delta R = R - R_o$. The sensing elements of the RTDs are commercially available in a variety of forms and sizes. Embedded type and surface type are two common types of RTDs. In the embedded type, the sensing element (a high purity platinum wire wound on a ceramic core) is protected , against environmental corrosive effects by an air tight sheath of steel, glass or ceramic. The surface type RTDs, on the other hand, utilize either a thin wire element or a thin filament element, resembling an ESG, which is surface bonded to the monitored component.

The output from an RTD can be easily monitored using a Wheatstone bridge and converted into a voltage signal, similar to that of an ESG. Common errors encountered during the use of RTDs are self heating and sensitivity of RTD to mechanical strain of the monitored component. Self heating can be minimized by limiting power dissipation in the RTD. The changes caused by mechanical strain in the structure are negligible due to the extremely low sensitivity of the RTDs to strain as compared to temperature. Typically, a nickel based RTD exhibits an apparent temperature change of 1.7^{o}C when subjected to an axial strain of 1000 μm/m. However, RTDs tend to be unstable when the upper temperature limit of the sensor is exceeded. This is not a problem for civil-structures where temperatures are not expected to exceed 50-60^{o}C at the most.

2.5.3 Thermistors

Thermistors are temperature sensitive resistors, similar to the RTDs, but fabricated from semiconducting materials, such as the oxides of nickel, cobalt or manganese or the sulphides of iron, aluminium or copper. However, unlike RTDs, their resistance decreases with increase in temperature and is governed according to the following relationship

$$R / R_o = e^{\beta(1/T - 1/T_o)} \tag{23}$$

where β is a material constant ranging from 3000K to 5000K, T the temperature to be measured and T_o the reference temperature, both on absolute scale. R is the resistance at temperature T and R_o at temperature T_o. Commercial thermistors are available in the form of beads (0.125-1.5mm diameter), hermetically sealed with a glass coating. As compared to RTDs, thermistors are more miniaturized, more sensitive, more stable and can be used over

large temperature ranges. Wheatstone bridge circuits can be utilized to automatically measure resistance changes in thermistors resulting from any temperature variations.

2.5.4 Thermocouples

Temperature measurement by thermocouples is based on the Seebeck effect, which results in the generation of a thermoelectric potential when two dissimilar metals are joined together, forming a junction. Typical commercial thermocouples are fabricated by joining two wires of dissimilar alloys (such as iron-constantan and copper-constantan), in an arrangement shown in Fig. 12. When temperature difference is created between the junctions T_1 and T_2 (by maintaining them at temperatures T_1 and T_2 respectively), diffusion of electrons occurs across the interface, thereby generating an electric field across the terminals P and Q. This voltage provides a measure of the temperature difference (T_1-T_2). The voltage across the terminals of a thermocouple is given by the equation

$$V = C_1(T_1 - T_2) + C_2(T_1^2 - T_2^2) \tag{24}$$

where T_1 and T_2 are the junction temperatures, and C_1 and C_2 the thermoelectric constants. In order to measure the unknown temperature T_1, the other junction must be maintained at a known constant temperature T_2. Four commonly used techniques for this purpose are: (i) ice water bath, (ii) thermoelectric refrigeration, (iii) electric bridge, and (iv) electric oven. Maintaining constant temperature is one of the drawbacks of employing thermocouples in the underground structures. Moyo (2002) reported extensive temperature measurements for the condition assessment of the bridge linking Singapore to Malaysia using thermocouples. The data was useful in understanding changes in structural dynamic response on account of temperature variations.

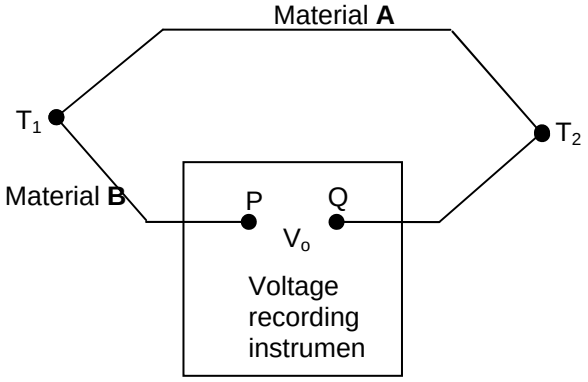

Fig. 12 A thermocouple circuit.

2.5.5 Piezo-Impedance Transducers

Unlike the transducers described above, piezo-impedance transducers are relatively new type of sensors, barely ten years old. They do not measure any direct physical parameter like stresses, strains or temperatures. Rather, they are capable of extracting a signature of the host structure by which any structural damages can be detected at the incipient stage. The technique utilizing the piezo-impedance transducers is commonly known as the electro-mechanical impedance (EMI) technique. Piezo-impedance transducers are made up of piezoelectric materials, such as lead zirconate titanate (acronymed PZT), and referred to as piezoceramic patches or PZT patches in the literature. Fig. 13(a) shows a typical commercially available PZT transducer, suitable for use as a piezo-impedance transducer.

The piezoceramic materials generate surface charges in response to an applied mechanical stresses. Conversely, they undergo mechanical deformations in response to the applied electric fields. In the EMI technique, the PZT patch is bonded to the surface of the monitored structure using a high-strength epoxy adhesive and electrically excited using an impedance analyzer. In this configuration, the patch (length $2l$, width w and thickness h) behaves as a thin bar undergoing axial vibration, as shown in Fig. 13(b). A mechanistic model of the system is shown in Fig. 13(c), where the structure has been replaced by two mechanical impedances Z. The complex electro-mechanical admittance $\overline{Y}$ (inverse of electrical impedance), of the coupled system shown in this figure can be derived as (Liang et al., 1994)

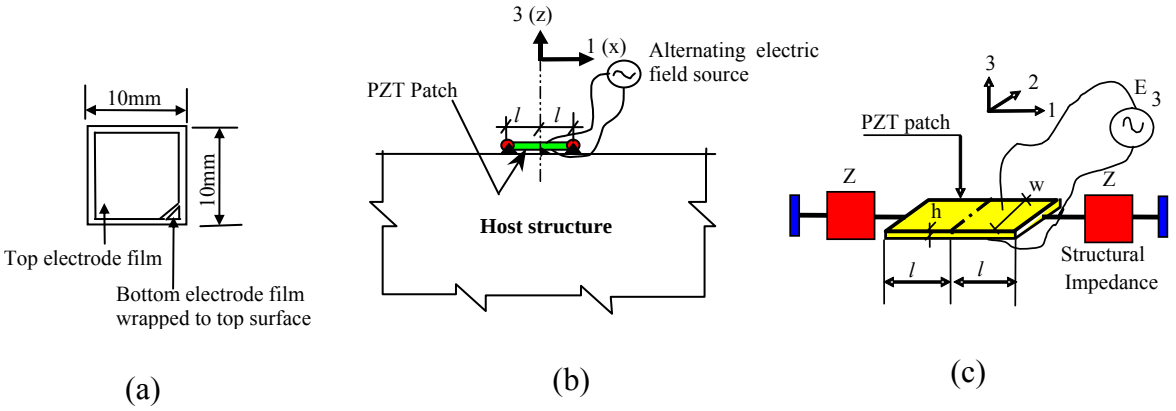

Fig. 13 (a) A commercial PZT patch.
(b) Principle of EMI technique.
(c) Equivalent model of system.

$$\overline{Y} = 2\omega j \frac{wl}{h}\left[\overline{\varepsilon_{33}^{T}} + \left(\frac{Z_a}{Z+Z_a}\right) d_{31}^2 \overline{Y^E}\left(\frac{\tan \kappa l}{\kappa l}\right) - d_{31}^2 \overline{Y^E}\right] \tag{25}$$

where d_{31} is the piezoelectric strain coefficient, $\overline{Y^E}$ the complex Young's modulus of the PZT patch at constant electric field, $\overline{\varepsilon_{33}^{T}}$ the complex electric permittivity of the PZT material at constant stress, Z_a the mechanical impedance of the PZT patch, ω the angular frequency, and κ the wave number.

The electromechanical coupling represented by Eq. (25) is utilized in damage detection in the EMI technique. The mechanical impedance Z in this equation is a function of the structural parameters, i.e., the stiffness, the damping and the mass. Any damage to the structure will cause these parameters to change, and hence changes the drive point mechanical impedance Z. Consequently, as can be seen from Eq. (25), the electromechanical admittance, $\overline{Y}$, will undergo change, and this serves as an indicator of the state of health of the structure.

The EMI technique has attracted intensive research during the last eight years. It has several advantages over the conventional load/ stress/ strain measurement based techniques, since it does not warrant any complex analytical/ numerical modelling of the monitored structure. It employs low-cost and low-power demanding transducers, which can be non-intrusively bonded to the structure and can be interrogated without removal of any finishes. Neither complex data processing nor any expensive hardware is necessary. By means of an array of such transducers, damage location can be easily identified (Soh et al., 2000). The technique has far greater sensitivity to damages than the global methods. Many proof of concept non-destructive evaluation (NDE) applications of the EMI technique have been reported in the literature (Sun et al., 1995; Ayres et al., 1998; Soh et al., 2000; Bhalla and Soh, 2004a).

Although the EMI technique is extremely sensitive in detecting damages, issues such as sensor packaging, instrumentation and long term protection are not yet standardized. Special considerations are called for in applying the EMI technique on underground structures. A comprehensive research programme is currently underway at NTU for developing low-cost practical SHM systems based on the EMI technique. This includes the development of realistic PZT-structure phenomenological models (Bhalla and Soh, 2003; 2004b, 2004c; Yang et al., 2005) as well as the development of damage localization and quantification algorithms (Xu et al., 2004; Naidu and Soh, 2004). Research groups in the

USA are carrying out active research for the development of low-cost and portable signature acquisition systems and wireless monitoring (Park et al., 2003; Peairs et al., 2004) which will make the technique more economical and standardized in the near future.

8. REFERENCES

Aktan, A. E., Helmicki, A. J. and Hunt, V. J. 1998. Issues in health monitoring for intelligent infrastructure. Smart Materials and Structures 7, 674-692.

Aktan, A. E., Catbas, F. N., Grimmelsman, K. A. and Tsikos, C. J. 2000. Issues in infrastructure health monitoring for management. Journal of Engineering Mechanics, ASCE 126, 711-724.

Ayres, J. W., Lalande, F., Chaudhry, Z. and Rogers, C. A. 1998. Qualitative impedance-based health monitoring of civil infrastructures. Smart Materials and Structures 7, 599-605.

Bakker, K. J. 2000. Soil retaining structures: development of models for structural analysis. Ph. D. thesis, Delfts University of Technology, Netherlands.

Batten, M., Boorman, R. and Leiper, Q. 1999. Use of vibrating wire strain gauges to measure loads in tubular steel props supporting deep retaining walls. Proceeding, Institution of Civil Engineers, Geotechnical Engineering 137, 3-13.

Bhalla, S. and Soh, C. K. 2003. Structural impedance based damage diagnosis by piezo-transducers. Earthquake Engineering and Structural Dynamics 32, 1897-1916.

Bhalla, S. and Soh, C. K. 2004a. High frequency piezoelectric signatures for diagnosis of seismic/ blast induced structural damages. NDT&E International 37, 23-33.

Bhalla, S. and Soh, C. K. 2004b. Structural health monitoring by piezo-impedance transducers. Part I : Modeling. Journal of Aerospace Engineering, ASCE 17, No. 4, pp. 154-165.

Bhalla, S. and Soh, C. K. 2004c. Structural health monitoring by piezo-impedance transducers. Part II : Applications. Journal of Aerospace Engineering, ASCE 17, No. 4, pp. 166-175.

Boller C. 2002. Structural health management of ageing aircraft and other infrastructure. Monograph on Structural Health Monitoring, Institute of Smart Structures and Systems (ISSS), Bangalore, 1-59.

Brownjohn, J. M. W., Moyo, P. Rizos, C. and Chuan, T. S. 2003a. Practical issues in using novel sensors in SHM of civil infrastructure: problems and solutions in implementation of GPS and fibre optics. Proceedings, 4th International Workshop on Structural Health Monitoring, September 15-17, Stanford University, California, 499-506.

Brownjohn J. M. W., Moyo, P., Omenzetter, P. and Lu, Y. 2003b. Assessment of highway bridge upgrading by dynamic testing and finite-element model updating. Journal of Bridge Engineering, ASCE 8, 499-506.

Clough, R. and Penzien, J. 1993. Dynamics of Structures, McGraw Hill, Singapore.

Coutts, D. R., Wang, J. and Cai, J. G. 2001. Monitoring and analysis of results for two strutted deep excavations using vibrating wire strain gauges. Tunnelling and Underground Space Technology 16, 87-92.

Dally, J. W., Riley, W. F. and McConnell, K. G. 1984. Instrumentation for engineering measurements, Wiley, New York.

Farrar, C. R. and Jauregui, D. A. 1998. Comparative study of damage identification algorithms applied to a bridge: I. Experiment. Smart Materials and Structures 7, 704-719.

Goel, R. K. 2001. Status of tunnelling and underground construction activities and technologies in India. Tunnelling and Underground Space Technology 16, 63-75.

Inaudi, D., Elamari, A., Pflug, L., Gisin, N., Breguet, J. and Vurpillot, S. 1994. Low-coherence deformation sensors for the monitoring of civil engineering structures. Sensors and Actuators 44, 125-130.

Inaudi, D., Vulliet, L., Pflug, L., Vurpillot, S. and Wyser, A. 1995. Low-coherence sensors for the monitoring of underground works. Proceeding, North American Conference on Smart Structures and Materials, San Diego, 2444, 171-178.

Liang, C., Sun, F. P. and Rogers, C. A. 1994. Coupled electro-mechanical analysis of adaptive material systems- determination of the actuator power consumption and system energy transfer. Journal of Intelligent Material Systems and Structures 5, 12-20.

Liu, J.-G., Hattenberger, C. S. and Borm, G. 2002. Dynamic strain measurement with a fibre Bragg grating sensor system. Measurement 32, 151-161.

Lynch, J. P., Partridge, A., Law, K. H., Kenny, T. W., Kiremidjian, A. S. and Carryer, E. 2003. Design of piezoresistive MEMS-based accelerometer for integration with wireless sensing unit for structural monitoring. Journal of Aerospace Engineering, ASCE 16, 108-114.

Moyo, P. 2002. Structural performance monitoring and health assessment of highway bridges. Ph.D. Thesis, Nanyang Technological University, Singapore.

Naidu, A. S. K. and Soh, C. K. 2004. Damage severity and propagation characterization with admittance signatures of piezo transducers. Smart Materials and Structures 13, 393–403.

Ng, S. L., Tjin, S. C., Xie, T. Q. and Soo, K. T. 1998. Side-projected fiber-optic velocity sensors. IEEE Photonics Technology Letters 10, 249-251.

Oosterhout, G. P. C. van. 2003. Recent Dutch experiences in developing structural monitoring systems for shield driven tunnels. HERON, 48, 65-78.

Pandey, A. K. and Biswas, M. 1994. Damage detection in structures using changes in flexibility. Journal of Sound and Vibration 169, 3-17.

Park, G., Cudney, H. H. and Inman, D. J. 2000. Impedance-based health monitoring of civil structural components. Journal of Infrastructure Systems, ASCE 6, 153-160.

Park, G., Sohn, H., Farrar, C. R. and Inman, D. J. 2003. Overview of piezoelectric impedance-based health monitoring and path forward. The Shock and Vibration Digest 35, 451-463.

Peairs, D. M., Park, G. and Inman, D. J. 2004. Improving accessibility of the impedance-based structural health monitoring method. Journal of Intelligent Material Systems and Structures 15, 129-139.

RS Components 2004. Northands, UK, http://www.rs-componenets.com

Sanayei, M. and Saletnik, M. J. 1996. Parameter estimation of structures from static strain measurements. I: Formulation. Journal of Structural Engineering, ASCE 122, 555-562.

Sharma, J. S., Hefny, A. M., Zhao, J. and Chan, C. W. 2001. Effect of large excavation on deformation of adjacent MRT tunnels. Tunnelling and Underground Space Technology 16, 93-98.

Soh, C. K., Tseng, K. K. H., Bhalla, S. and Gupta, A. 2000. Performance of smart piezoceramic patches in health monitoring of a RC Bridge. Smart Materials and Structures 9, 533-542.

Soh, C. K. and Bhalla, S. 2004. Calibration of piezo-impedance transducers for strength prediction and damage assessment of concrete. Smart Materials and Structures, in press.

Storoy, H., Saether, J. and Johannessen, K. 1997. Fiber optic condition monitoring during a full scale destructive bridge test. Journal of Intelligent Material Systems and Structures 8, 633-643.

Sun, F. P., Chaudhry, Z., Rogers, C. A., Majmundar, M. and Liang, C. 1995. Automated real-time structure health monitoring via signature pattern recognition. Proceedings, SPIE Conference on Smart Structures and Materials, San Diego, California, Feb.27-Mar1, 2443, 236-247.

Tjin, S. C., Hao, J. Z., Lam, Y. Z., Ho, Y. C. and Ng, B. K. 2001. A pressure sensor using fiber Bragg grating. Fiber and Integrated Optics 20, 59-69.

Tjin, S. C., Rupali, S., Moyo P., Brownjohn, J. M. W. and Ngo, N. Q. 2002. Application of fibre Bragg grating based sensors for civil infrastructure health monitoring. Proceedings, ISSS-SPIE International Conference on Smart Materials, Structures and Systems, Bangalore, 12-14 December, 683-690.

Valliappan, S. and Pham, T. D. 1993. Fuzzy finite element analysis of a foundation on an elastic medium. International Journal for Numerical and Analytical Methods on Geomechanics 17, 771-789.

Wu, C. Q., Hao, H. and Zhou, Y. X. 1999. Fuzzy-random probabilistic analysis of rock mass responses to explosive loads. Computers and Geotechnics 25(4), 205-225.

Xu, J. F., Yang, Y. W. and Soh, C. K. 2004. EM impedance-based structural health monitoring with evolutionary programming. Journal of Aerospace Engineering, ASCE 17, No. 4, in press.

Yang, Y. W., Xu, J. F. and Soh, C. K. 2005. A generic impedance-based model for structure-PZT interacting System. Journal of Aerospace Engineering, ASCE 18, No. 1, in press.

Zhao, J., Liu, Q., Lee, K. W., Choa, V. and Teh, C. I. 1999. Underground cavern development in the Jurong sedimentary rock formation. Tunnelling and Underground Space Technology 14, 449-459.

Zhao, J., Cai, J. G., Tunbridge, L., Song, H. W., Zhang, X. H. and Zhao, X. B. 2002. Results of rock cavern monitoring and assessment of cavern stability. Technical report for NTU-DSTA Joint R&D Project on instrumentation and monitoring of rock caverns during construction and operation.

Zhao, J. 2003. The underground science city. International Tunnelling Association (http://www.ita-aites.org/cms/335.html)